

# Global Biogeochemical Cycles

## RESEARCH ARTICLE

10.1029/2019GB006430

### Special Section:

Carbon cycling in tidal wetlands and estuaries of the contiguous United States

### Key Points:

- We present a complete carbon budget for the largest brackish tidal marsh in the Pacific United States
- Direct and indirect measurement showed 47% to 59% of fixed carbon is stored on site and most loss is through inorganic carbon export
- A compilation of global data sets showed lateral loss larger term in coastal wetland carbon budgets, relative to other terrestrial systems

### Supporting Information:

- Supporting Information S1

### Correspondence to:

M. J. Bogard,  
matthew.bogard@uleth.ca

### Citation:

Bogard, M. J., Bergamaschi, B. A., Butman, D. E., Anderson, F., Knox, S. H., & Windham-Myers, L. (2020). Hydrologic export is a major component of coastal wetland carbon budgets. *Global Biogeochemical Cycles*, 34, e2019GB006430. <https://doi.org/10.1029/2019GB006430>

Received 17 SEP 2019

Accepted 3 JUN 2020

Accepted article online 7 JUL 2020

## Hydrologic Export Is a Major Component of Coastal Wetland Carbon Budgets

Matthew J. Bogard<sup>1,2</sup> , Brian A. Bergamaschi<sup>3</sup> , David E. Butman<sup>1,4</sup> , Frank Anderson<sup>3</sup> , Sara H. Knox<sup>5</sup> , and Lisamarie Windham-Myers<sup>6</sup> 

<sup>1</sup>School of Environmental and Forest Sciences, University of Washington, Seattle, WA, USA, <sup>2</sup>Now at: Department of Biological Sciences, University of Lethbridge, Lethbridge, Alberta, Canada, <sup>3</sup>California Water Science Center, U.S. Geological Survey, Sacramento, CA, USA, <sup>4</sup>Department of Civil and Environmental Engineering, University of Washington, Seattle, WA, USA, <sup>5</sup>Department of Geography, The University of British Columbia, Vancouver, British Columbia, Canada, <sup>6</sup>National Research Program, U.S. Geological Survey, Menlo Park, CA, USA

**Abstract** Coastal wetlands are among the most productive habitats on Earth and sequester globally significant amounts of atmospheric carbon (C). Extreme rates of soil C accumulation are widely assumed to reflect efficient C storage. Yet the fraction of wetland C lost via hydrologic export has not been directly quantified, since comprehensive budgets including direct estimates of lateral C loss are lacking. We present a complete net ecosystem C budget (NECB), demonstrating that lateral losses of C are a major component of the NECB for the largest stable brackish tidal marsh on the U.S. Pacific coast. Mean annual net ecosystem exchange of CO<sub>2</sub> with the atmosphere (NEE =  $-185 \text{ g C m}^{-2} \text{ year}^{-1}$ , negative NEE denoting ecosystem uptake) was compared to long-term soil C burial ( $87\text{--}110 \text{ g C m}^{-2} \text{ year}^{-1}$ ), suggesting only 47–59% of fixed atmospheric C accumulates in soils. Consistently, direct monitoring in 2017–2018 showed NEE of  $-255 \text{ g C m}^{-2} \text{ year}^{-1}$ , and hydrologic export of  $105 \text{ g C m}^{-2} \text{ year}^{-1}$  (59% of NEE remaining on site). Despite their high C sequestration capacity, lateral losses from coastal wetlands are typically a larger fraction of the NECB when compared to other terrestrial ecosystems. Loss of inorganic C (the least measured NECB term) was 91% of hydrologic export and may be the most important term limiting C sequestration. The high productivity of coastal wetlands thus serves a dual function of C burial and estuarine export, and the multiple fates of fixed C must be considered when evaluating wetland capacity for C sequestration.

## 1. Introduction

Coastal wetlands are one of the most economically important ecosystems globally, providing critical habitat and resources for commercially important species, water purification via filtration of aquatic nutrients and toxins, and protection from flooding and storms (Barbier et al., 2011; Boesch & Turner, 1984; Worm et al., 2006). Coastal wetlands contribute disproportionately to the global carbon (C) cycle through intense plant uptake of atmospheric CO<sub>2</sub> and soil C sequestration (Duarte et al., 2005, 2013; Najjar et al., 2018; Windham-Myers et al., 2018), burying 30 to 50 times more C per unit area in soil layers than forests, despite covering only ~3% of the surface area relative to forested terrestrial landscapes (Duarte et al., 2013). Coastal habitats are also among the most threatened ecosystem types, and although these services are collectively valued at  $\sim \$10,000 \text{ USD ha}^{-1} \text{ year}^{-1}$ , human-driven sea level rise (SLR), eutrophication, and land conversion have resulted in the loss and degradation of up to 50% of global coastal wetland extent (Barbier et al., 2011; Worm et al., 2006). For these reasons, the protection and restoration of coastal vegetated habitats have been widely regarded as an efficient and cost-effective tool to combat human-driven CO<sub>2</sub> release and climatic change (Duarte et al., 2013; McLeod et al., 2011; Nellemann et al., 2009; Xiao et al., 2019).

Our understanding of coastal wetland C cycling is hampered by a weak appreciation for lateral exchanges with adjacent marine environments (Bauer et al., 2013; Maher et al., 2018; McLeod et al., 2011; Najjar et al., 2018; Windham-Myers et al., 2018). Coastal wetlands are widely regarded as sites of extreme efficiency for C sequestration, owing to both their capacity to trap lateral imports of riverine and marine C, plus their unique capacity to overcome soil C saturation through vertical accretion (McLeod

et al., 2011). This efficiency of C capture, though not empirically constrained (Bauer et al., 2013; Cai, 2011), is a key assumption pertaining to the valuation of ecosystem services derived from coastal wetland C capture, particularly regarding their net capacity as CO<sub>2</sub> sinks and in land mass accretion in the face of ongoing anthropogenically driven SLR (Duarte et al., 2013; Kirwan & Megonigal, 2013; Maher et al., 2018; McLeod et al., 2011).

Although high rates of coastal wetland C sequestration are well established in the literature, recent reports of large lateral C exports from coastal wetlands may challenge the assumed efficiency of this C sequestration. Direct and indirect estimates of exchange between wetlands (both marshes and mangrove forests) and coastal waters have demonstrated that lateral fluxes are often on the same order of magnitude as vertical exchanges (Cai, 2011; Dittmar et al., 2006; Forbrich et al., 2018; Ho et al., 2017; Maher et al., 2018; Santos et al., 2019; Troxler, 2013; Wang et al., 2016, 2018). Although estimates of lateral exports of dissolved inorganic C (DIC) are sparse (Bouillon et al., 2003; Cai, 2011; Chu et al., 2018; Ho et al., 2017; Maher et al., 2018; McLeod et al., 2011; Wang et al., 2018), novel, high-resolution methods show DIC export may greatly exceed previous estimates (Wang et al., 2016) and that these fluxes arise from intense soil respiration plus land-water exchanges linked to tidal pumping (Cai, 2011; Santos et al., 2019; Wang et al., 2016). Lateral DIC exports may represent an overlooked sink of wetland-derived C, given that a fraction of this C may be retained over geologic timescales in the open ocean (Bouillon, Borges, et al., 2008; Maher et al., 2018). However, extreme intertidal variability in net DIC exchange suggests that low-frequency sampling (e.g., a few tidal cycles) likely has large associated uncertainties when extrapolated to annual timescales (Chu et al., 2018; Wang et al., 2016). Lateral exports of dissolved organic C (DOC) from coastal marshes have been estimated more frequently than DIC (Bergamaschi et al., 2011; Bergamaschi, Fleck, et al., 2012; Bouillon, Borges, et al., 2008; Cai, 2011; Dittmar et al., 2001, 2006; Downing et al., 2009; Santos et al., 2019), and marsh-estuary OC exchanges may be several times greater than riverine inputs in some regions (Cai, 2011), but not in others (Jassby et al., 1993). Comprehensive budgets combining OC and DIC exports over annual or longer timescales are near absent (Santos et al., 2019; Wang et al., 2016), but large overall lateral C exports have been inferred by indirect estimates subtracting vegetation net C uptake from soil C burial (Feijtel et al., 1985; Forbrich et al., 2018; Troxler, 2013; Webb et al., 2018). Ultimately, direct and simultaneous measurement of both DIC and OC at a high temporal resolution and across complete annual cycles is required to better define the magnitude and chemical makeup of coastal wetland lateral C exports. Such information will contribute to better understanding the ratio of organic to inorganic C exports, which has implications for defining the fate of exported wetland C, for constraining patterns of coastal ocean CO<sub>2</sub> emissions, and for understanding coastal ecosystem buffering capacity and resilience to acidification (Cai, 2011; Tank et al., 2012).

Site-specific net ecosystem C budgets (NECBs; Chapin et al., 2006) linking terrestrial C capture to aquatic C exports are needed to fully resolve tidal marsh C budgets and to parameterize larger-scale biogeochemical modeling efforts (Butman et al., 2016; Cai, 2011; Najjar et al., 2018; Webb et al., 2018; Windham-Myers et al., 2018). Extreme environmental variability over multiple timescales in coastal marsh environments necessitates both high-resolution and longer-term (i.e., annual to multiyear) data sets to accurately capture net C exchange patterns over representative timeframes (Feijtel et al., 1985; Forbrich et al., 2018; Troxler, 2013). Unfortunately, integrative NECBs are rare for all ecosystem types, especially tidal wetlands (Webb et al., 2018), and our understanding of these habitats lag behind other environments. Few studies consider lateral DIC and OC fluxes simultaneously, and fewer still consider them in the context of vertical terrestrial flux, making it difficult to constrain coastal wetland C cycling. Here we address this issue by characterizing the C cycle of the most extensive brackish marsh complex in California, USA (Figure S1). We combine published soil burial (Callaway et al., 2012) and terrestrial eddy covariance (EC) measurements (Knox et al., 2018) with new, high- and low-frequency aquatic measurements to produce the first complete tidal marsh NECB. Given that few tidal wetland NECBs exist (Feijtel et al., 1985; Forbrich et al., 2018; Troxler, 2013; Webb et al., 2018), and none include direct, high-resolution measurements of lateral C flux, these findings provide important ecological and biogeochemical insights into coastal wetland processes. They also provide a comprehensive and scalable evaluation of coastal wetland C cycling that will help to constrain C budgets at coastal margins (Bauer et al., 2013; Cai, 2011; Jassby et al., 1993; Maher et al., 2018; Najjar et al., 2018; Wang et al., 2016; Windham-Myers et al., 2018; Xiao et al., 2019).

## 2. Methods

### 2.1. Study Site

As previously detailed (Knox et al., 2018), the Suisun Wetland complex is a 4.57 km<sup>2</sup> brackish tidal marsh located in the San Francisco Bay National Estuarine Research Reserve (SFBNERR) in Suisun Bay, CA, USA (Figure S1 in the supporting information). The complex is classified as high marsh (irregularly flooded, National Wetland Inventory, U.S. Fish and Wildlife Service), the most common tidal classification (58%) of U.S. estuarine wetlands. The region experiences a Mediterranean-type climate with hot, dry summers and cool, wet winters (Knox et al., 2018). The San Francisco Estuary exhibits mixed semidiurnal tides with two unequal high tides and two unequal low tides per 24.84 hr lunar day (Enright et al., 2013). In First Mallard Slough (FM), where aquatic measurements were made (see below), the site is characterized as mesohaline, with a mean tidal range of 1.72 m (Callaway et al., 2012). Only about 15% of high tides flood over channel banks during spring tides, while a smaller percentage of high tides flood the marsh plain (Enright et al., 2013). The regional water surface elevation varies by season and experiences the highest stages during winter, when high river flows predominantly occur (Bergamaschi et al., 2011).

### 2.2. Vertical C Exchange

In the spring of 2014, the USGS, working in conjunction with the SFBNERR and Solano Land Trust, established an EC flux tower on the edge of the Suisun Marsh in the San Francisco Bay, just south of Rush Ranch and approximately 60 km northeast of San Francisco. The site and monitoring setup have been fully described elsewhere (Knox et al., 2018). The EC flux tower provides high-frequency (10 Hz) continuous measurements of temperature, water vapor, and CO<sub>2</sub> concentrations along with three-dimensional measurements of wind speeds to quantify the net exchange of CO<sub>2</sub> and sensible and latent heat between the marsh vegetation and the atmosphere (Balocchi, 2003) (Figure S1). Thirty minute fluxes of C, water and energy were calculated using MATLAB software (MathWorks Inc., 2016, Version 9.1.0, Mathworks Inc., Natick, MA, USA) developed by the University of California, Berkeley Biometeorology Group, with standard corrections applied (Knox et al., 2018). As previously outlined (Knox et al., 2018), an artificial neural network (ANN) technique was used to both gap-fill missing fluxes of CO<sub>2</sub> and to estimate annual gap-filled and random error uncertainty. Gap filling relied on model inputs based on season, time of day, net radiation, water temperature, air temperature, and vapor pressure deficit (Moffat et al., 2007). We combined EC-derived net ecosystem exchange (NEE, where negative denotes net ecosystem CO<sub>2</sub> uptake) data with two different published estimates of C burial rates from the Rush Ranch wetland complex, using <sup>210</sup>Pb and <sup>137</sup>Cs radio-dating techniques (Callaway et al., 2012).

### 2.3. Manual Aquatic Sampling

Water samples were manually collected to accurately model sensor-based estimates of DOC and DIC. Samples for DOC were collected on 27 June 2018 by pumping water from ~1.5 m depth across a 0.2 µm filter into amber glass vials that were transported on ice to the lab then stored chilled (4°C) and analyzed within 24 hr using high-temperature combustion oxidation (Shimadzu TOC-VCPh). Samples for DIC analysis were collected on three occasions in 2018: Two samples were collected on 21 May, from high to low water on ebb tide at 8:30 and 13:00, respectively. Four samples were collected on 27 June, from low to high water levels during flood tide at 9:30, 11:30, 13:30, and 15:30. May and June samples were collected by pumping water into glass bottles, preserving samples with 100 µl of ZnCl<sub>2</sub>, then capping bottles free of air with grease-lined glass stoppers. On 4 and 5 October, an additional 25 samples were collected at 30 min intervals (from high to low water on ebb tide, from 18:30 until 06:30). October samples were collected by pumping water; filtered at coarse pore size, from ~1.5 m depth into 375 ml amber bottles to near capacity; fixed with 80 µl of HgCl<sub>2</sub> preservative; and then immediately crimp sealed. In all cases, bottles were triple-rinsed then allowed to overflow for a total of three to four times the volume of the bottle before sealing. Samples from May and June were analyzed at the School of Oceanography, University of Washington, using a coulometer (UIC, Inc.) coupled to a DIC acidification system (Marianda VINDTA), following standard methods (Dickson et al., 2007). Samples collected in October were analyzed at Oregon State University, and total alkalinity was calculated from the combination of DIC and partial pressure of CO<sub>2</sub>, following standard methods (Bandstra et al., 2006). Both total alkalinity and DIC estimates were paired with salinity and water temperature estimates to calculate the saturation state of aragonite and calcite ( $\Omega_a$  and  $\Omega_c$ , respectively), as detailed

in Waldbusser et al. (2015). Given the high precision of DIC measurements, and the general agreement between methods over long gradients spanning low to high water stage (data not shown), we combined both data sets in our multiple regression analyses.

#### 2.4. Aquatic Sensor Deployments

A suite of continuous, sensor-based measurements of both physicochemical and hydrodynamic conditions were made in order to quantify high-frequency changes in First Mallard Slough (Figure S1; U.S. Geological Survey stn. 381142122015801). Estimates of water temperature, specific conductivity, salinity, dissolved oxygen, water depth, pH, fluorescent dissolved organic carbon (*f*DOM), and turbidity were made using an YSI EXO2 combination probe (Campbell Scientific). Sensor deployment protocols are fully described in earlier work (Downing et al., 2009). Raw *f*DOM measurements were made on unfiltered water, which were subsequently corrected for temperature, inner filter, and turbidity effects (Downing et al., 2012). Turbidity corrections were based on laboratory-established relationships between turbidity and *f*DOM (Downing et al., 2012). This approach is suitable at the low turbidity levels occurring in First Mallard Slough (all turbidity values <245 FNU and most typically <100 FNU) (Saraceno et al., 2017). Salinity was calculated from specific conductivity, water temperature, and pressure using the “swSCTp” function in the R package “oce” (<https://dankelley.github.io/oce>). For each measured parameter, small measurement gaps in each series were filled using a linear interpolation method within the “na.interpolation” function.

#### 2.5. Hydrodynamic Measurements and Calculations

Water height and averaged water velocities were measured with an upward-looking acoustic Doppler velocity meter (ADVM; Sontek Argonaut XR, Sontek) deployed on the First Mallard channel bed near the NERR monitoring station (Figure S1), as previously described (Bergamaschi et al., 2011; Ganju et al., 2005). Measurements were recorded every 15 min for 6 min. To calculate rates of discharge from measured water height and average water velocity, surveys were conducted with a downward-looking acoustic Doppler profiler to relate the cross-sectional area to water height and measured velocity to the channel-wide average velocity. In cases where water import and exports did not balance for a given tidal cycle, the water balance was forced to closure following existing methods (Bergamaschi et al., 2011). It is unlikely that this imbalance was related to effects of evapotranspiration (ET). The spatial extent of surface flooding is very small, so ET is expected to be a small fraction of the budget. This has been demonstrated in a similar, nearby tule tidal system (Browns Island), where ET was a minor component in fluxes measured (Bergamaschi, Fleck, et al., 2012). A salt balance calculation (Ganju, 2011) was used to evaluate the potential contribution of groundwater inputs. Annually averaged groundwater inputs were  $0.07 \text{ m}^3 \text{ s}^{-1}$ , with a peak of  $\sim 1.8 \text{ m}^3 \text{ s}^{-1}$  (data not shown), similar to previous observations (Ganju, 2011), and below the uncertainty of the discharge measurement itself, and thus too small to affect flux calculations. This salt balance approach further confirms that effects of ET were minimal and there is no major underlying bias in our modeling of the hydrologic cycle in the system.

#### 2.6. Computation of Lateral Flux of C Species and Associated Error

Continuous estimates of lateral flux of C species were made at 15 min time intervals by multiplying total water exchange by modeled concentrations of either DIC or DOC. We assumed no overbanking water losses occurred in the channel. Concentrations of DOC were modeled from continuous measurements of *f*DOM based on the regression relationship established between discrete DOC samples and *f*DOM for First Mallard Slough (Figure S3). Concentrations of DIC were estimated using a multiple linear regression (MLR) modeling approach (Chu et al., 2018; Wang et al., 2016) (Figure S2). We explored the relationship between measured DIC and all sensor-based, empirically measured water quality parameters that could be used to predict DIC (full table with all predictors in Table S1), with the objective of maximizing the predictive capacity of the model (i.e., maximizing  $r^2$  value of model). Given that stage alone predicted 85% of variance in DIC concentrations, we sequentially explored the strength of models using stage plus one then two additional parameters (Table S1).

The flux of particulate organic carbon (POC) was derived from the continuous record of turbidity by using the turbidity : suspended sediment concentration (SSC) relationship (Buchanan & Morgan, 2014) and the Wt% OC reported by Bergamaschi et al. (2001). Calculating the POC fluxes using this method revealed they

**Table 1**

Net Ecosystem Carbon Budget (NECB) for Suisun Wetland Complex

Process	C flux (g C m <sup>-2</sup> year <sup>-1</sup> )	±1 SD	Range (min–max)	Uncertainty or error (%)	Reference
Indirect lat. flux estimate					
NEE (4 yr avg.)	-185	171			Bergamaschi and Windham-Myers (2018); Knox et al. (2018)
Long Term Burial	98.5		(87–110)		Callaway et al. (2012)
Export (by difference)	86.5		(75–98)		This study
Direct flux estimates from 1 September 2017 to 31 August 2018					
NEE	-254.5		36.7		This study
DIC export	95.7		7.5 ( $\pm 7.8\%$ )		This study
DOC export	9.7		2.2 ( $\pm 22.8\%$ )		This study
Total C export	105.4		25.4 ( $\pm 24.1\%$ )		This study

Note. Negative NEE denotes ecosystem uptake.

were far less than 1% of the calculated DOC flux and thus POC was neglected in subsequent calculations as it was judged to be within the measurement error (see below).

We calculated the error associated with annual flux estimates for DOC, DIC, and total C using a square root of the sum of squares approach, directly following earlier studies (Bergamaschi et al., 2011; Bergamaschi, Fleck, et al., 2012; Ganju et al., 2005). Calculations were made under the assumption that the error associated with individual measurements was uncorrelated. For DOC, laboratory measurement error was estimated to be  $\pm 1\%$  (Bergamaschi, Krabbenhoft, et al., 2012), and the root-mean-square error (RMSE) of prediction for the DOC versus fDOM linear model was  $\pm 0.63 \text{ mg L}^{-1}$  or 22% (Figure S3). For DIC, the laboratory measurement error was estimated as conservatively high at  $\pm 0.5\%$ , and the RMSE of prediction for the final regression model was  $1.81 \text{ mg L}^{-1}$ , or 5% (Figure S2; Table S1). For both DOC and DIC, the error in discharge estimates was previously estimated at 6% (Bergamaschi, Krabbenhoft, et al., 2012; Ganju et al., 2005). Final error estimates for DOC and DIC were 22.8% and 7.8%, respectively, and when combined as estimates of total dissolved C export, error was 24.2% (Table 1).

## 2.7. Tidal Footprint Estimations

An upper end estimate of the areal extent of tidal exchange was estimated from an existing method (Bergamaschi et al., 2011; Bergamaschi, Fleck, et al., 2012) using data from 15 June 2018, which was a period of extreme tidal water exchange and the highest water level periods of the annual sampling cycle. We estimated the planar surface of the marsh platform that was flooded by dividing the maximal change in known water height (1.3 m) and total water volume ( $3.85 \times 10^5 \text{ m}^3$ ), and correcting for soil porosity and moisture content using existing values from a nearby site with similar soil type (Bergamaschi et al., 2011, and references therein). We obtained an estimate of flooded land totaling  $\sim 0.53 \text{ km}^2$ . This calculation was validated by an independent mapping-based catchment delineation (Wang et al., 2016) (Figure S1).

## 2.8. Statistical Analyses

All statistical calculations were performed using the R software package (R-development-core-team, 2017). Major axis regression analysis was conducted in the “lmodel2” package (Legendre, 2013), while Pearson’s correlation and ordinary least squares bivariate and MLR analyses were performed with the R base program. Multiple regression models were evaluated based on their predictive strength and also their associated Akaike’s Information Criterion (AIC) value (Johnson & Omland, 2004). For evaluation of C flux data in our data compilation, a Shapiro-Wilk Normality Test was used to determine whether estimates of the fraction of NEP lost as lateral C export were normally distributed. Given the nonnormal distribution of data ( $W = 0.76634, p < 0.0001$ ), a Wilcoxon signed-rank test was used to compare fractions of NEP lost as lateral C export across coastal and inland ecosystems.

### 3. Results

#### 3.1. Time Series of Aquatic Conditions

Sensor-based measurements were obtained for a complete annual cycle at First Mallard Slough at the outflow of the Rush Ranch wetland site (Figure 1). Annually, water levels ranged between 6.7 and 9.0 m, reaching the lowest levels in winter 2017/2018 and highest levels in summer 2018 (Figure 1a). On a daily timeframe, water levels fluctuated by ~1.5 to 2 m (Figure 1a). Tidally driven flows ranged between ~40 and  $-30 \text{ m}^3 \text{ s}^{-1}$  (negative denotes influx into First Mallard Slough), with maxima and minima occurring in late spring and summer 2018 (Figure 1b). Annually, water temperatures ranged considerably, from  $7.1^\circ\text{C}$  in November and December 2017 to  $26.8^\circ\text{C}$  in late spring and summer 2018 (Figure 1c). Daily temperature changes spanned from  $\sim 1^\circ\text{C}$  changes in winter up to  $\sim 5^\circ\text{C}$  changes in summer 2018. Salinity (in practical salinity units, PSUs) also ranged considerably at the annual scale (Figure 1d), with highs of  $\sim 10$  PSU in Winter of 2017 and  $\sim 8$  PSU in June/July 2018 and lows reaching  $<2$  PSU in spring 2018. Suspended solid concentrations inferred from turbidity measurements (Figure 1e) were generally low, with all values  $<250$  formazin nephelometric units (FNUs) and most values  $<150$  and as low as 25 FNU. Average values of turbidity were lowest in fall 2017 and highest from March to July 2018. Daily ranges in turbidity values were typically between  $\sim 20$  to 80 FNU. Chlorophyll *a* concentrations, a proxy for phytoplankton biomass, were typically  $<20 \mu\text{g L}^{-1}$  but peaked on two separate bloom occasions to  $>70 \mu\text{g L}^{-1}$  between February and April 2018 (Figure 1f). Annually, fluorescent dissolved organic matter (*f*DOM) concentrations ranged from 22 to 227 Quinine sulfate equivalents (QSEs), with a distinct increase in December 2017 (Figure 1g). On daily scales, tidal exchanges of distinct water masses led to *f*DOM changes from  $\sim 50$  to over  $\sim 150$  QSE.

#### 3.2. Measuring and Modeling Aquatic C Concentrations

Samples collected in May, June, and October 2018 ranged in DIC concentration from 26.0 to  $44.0 \text{ mg L}^{-1}$ . To develop the best empirical model of aquatic DIC concentrations for application to the high-resolution data set (Figure 2a), manual samples of DIC were grouped with sensor data from equivalent time points to conduct a series of MLRs (full model comparisons in Table S1). The strongest individual predictor of DIC concentrations was water stage (Pearson's  $r = -0.92$ ,  $p < 0.0001$ ), yet comparisons using AIC indicated the most parsimonious model included stage, water temperature ( $^\circ\text{C}$ ), and salinity (PSU) ( $\text{DIC} = 114.75 - 8.04 \text{ stage} - 0.91 \text{ temperature} + 0.38 \text{ salinity}$ ;  $r^2 = 0.88$ ;  $p < 0.0001$ ; AIC = 130.65; Table S1; Figure S2). The predictive strength of this MLR model is closely in line with another, existing DIC MLR model derived from the combination of measured DIC and high-frequency environmental parameter measurements ( $r^2 = 0.91$ ; Chu et al., 2018). By applying the multiple regression model to high-frequency measurements of water height, salinity, and temperature (Figure 1), we modeled DIC concentrations at 15 min intervals for First Mallard Slough (Figure 2a). From September 2017 to January 2018, DIC concentrations increased from a low of  $\sim 25 \text{ mg L}^{-1}$  to a maximum of  $>55 \text{ mg L}^{-1}$ , before declining to lows of  $\sim 25 \text{ mg L}^{-1}$  again by summer 2018 (Figure 2a). On shorter, daily/tidal timescales, DIC concentrations ranged considerably, often by  $>15 \text{ mg L}^{-1}$  with high DIC waters peaking at ebbing tide and low values peaking during flooding tides, consistent with previous studies (Cai & Wang, 1998; Neubauer & Anderson, 2003; Santos et al., 2019; Wang et al., 2018).

To model high-frequency concentrations of DOC (Figure 2b), we used a major axis regression approach to model the relationship between measured DOC and fluorescent dissolved organic matter (*f*DOM) concentrations. Direct measurements of DOC from First Mallard Slough taken on 26 June 2018 spanned concentrations of 7.8 to  $12.9 \text{ mg L}^{-1}$ , and the corresponding *f*DOM measurements ranged from 109 to 180 QSE (Figure S3). These samples covered a wide, middle- to upper-end range of values of *f*DOM observed annually at our site (Figure 1g). We paired these data with other DOC and *f*DOM measurements from sites within the watershed (Bergamaschi et al., 2011; Downing et al., 2012) in order to expand the regression model to the lower ranges of DOC and *f*DOM. Overall, we found a strong linear relationship between *f*DOM and DOC (Figure S3;  $r^2 = 0.87$ ;  $p < 0.0001$ ;  $n = 440$ ;  $\text{DOC} = 0.071\text{fDOM} + 1.037$ ). Applying this model yielded high-frequency DOC concentrations ranging from  $\sim 2.5$  to  $16 \text{ mg L}^{-1}$  (Figure 2b). Seasonally, averaged DOC concentrations varied more frequently than for DIC, reaching lows of  $\sim 8$  (September 2017), increasing to  $\sim 11$  (January 2018), and then declining again to  $\sim 8 \text{ mg L}^{-1}$  (winter to early spring 2018) with a moderate increase by May 2018.

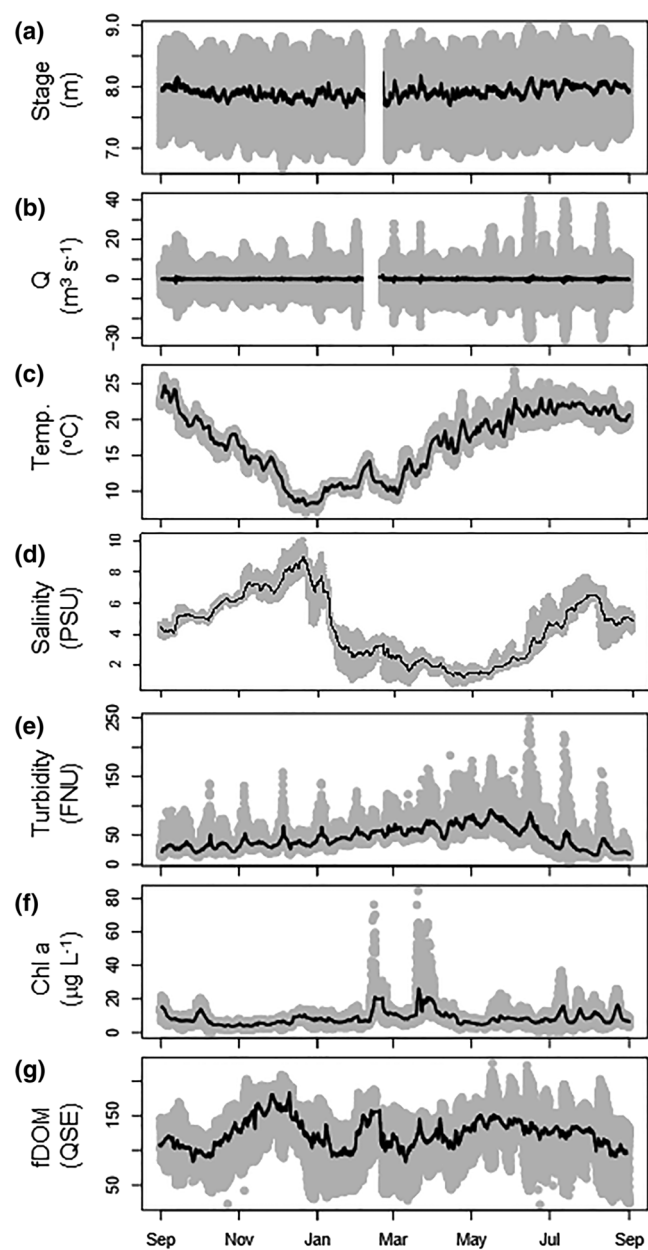


**Figure 1.** High-resolution time series of aquatic conditions in First Mallard Slough. Data were collected from 1 September 2017 to 31 August 2018 at 15 min intervals for (a) water surface height (stage), (b) the rate of discharge ( $Q$ ), (c) water temperature, (d) salinity, (e) turbidity, (f) chlorophyll  $a$  concentration, and (g) fluorescent dissolved organic matter. Gray points are individual measurements and solid black line denotes 24 hr moving average.

teral export agrees closely between approaches (41% and 47% for direct and indirect calculations, respectively; Table 1), such agreement between long term and our single year estimates might not be expected in other individual years, because marsh NEE (and possibly lateral C export) varies widely among years (but aquatic exports tend vary much less than NEE; Webb et al., 2018). The long-term average  $\text{CO}_2$  uptake rate used here was lower than the rate in the focal year in this study, reflecting years with extremely low NEE (i.e., less  $\text{CO}_2$  uptake) in the average NECB flux terms. This discrepancy highlights the need for longer-term (multiyear) perspectives when evaluating ecosystem C cycling capacities. Coastal wetlands have been hypothesized to efficiently trap C (McLeod et al., 2011), but our findings support past observations (Bouillon, Borges,

### 3.3. Patterns of Lateral Aquatic C Flux

The flux of individual C species (DIC and DOC) for each 15-min measurement interval was determined as the product of the rate of instantaneous flow ( $\text{m}^3 \text{s}^{-1}$ ; Figure 1b) and DIC or DOC concentration for the equivalent time point (Figures 2a and 2b), multiplied by 900 s. When summed at daily intervals, DIC fluxes showed a much wider range (from  $-2.6$  to  $2.9 \text{ Mg C day}^{-1}$ ) than did DOC (typically between  $-0.7$  and  $0.7 \text{ Mg C day}^{-1}$ ). Fluxes of each C constituent, normalized to an upper estimate of the footprint of marsh flooding, gave a conservative estimate of areal yields (Figures 2d and S1). In total, annual yields were  $95.7$  and  $9.7 \text{ g C m}^{-2} \text{ year}^{-1}$  for DIC and DOC, respectively (Figure 2d; Table 1).

### 3.4. High-Resolution Annual NECB for Suisun Marsh

The individual lateral fluxes summed to a total wetland C yield of  $105.4 \text{ g C m}^{-2} \text{ year}^{-1}$  (Figure 3; Table 1). The equivalent estimate of terrestrial net ecosystem C exchange (NEE) measured for the marsh was  $-254 \text{ g C m}^{-2} \text{ year}^{-1}$  for the same timeframe as aquatic flux measurements (September 2017 to September 2018; Figures 2d and 3; Table 1). Lateral exports of C represented 41.4% of the total annual terrestrial NEE for the complete annual cycle from September 2017 to September 2018.

## 4. Discussion

### 4.1. Lateral Loss: A Major Term in Suisun Marsh C Budget

Direct and indirect estimates confirm that hydrologic C export is a major component of the NECB for Suisun Marsh complex, which offsets net atmospheric C uptake to lower the overall proportion of onsite C sequestration. Direct estimates of lateral C flux agree with indirect estimates of marsh C export calculated as the difference between multiyear averaged ( $\pm 1 \text{ SD}$ ) terrestrial NEE ( $185 \pm 171 \text{ g C m}^{-2} \text{ year}^{-1}$ ) (Bergamaschi & Windham-Myers, 2018; Knox et al., 2018) and published, long-term (interdecadal) C burial rates for our site (Callaway et al., 2012) (Figure 3; Table 1). The rate of soil C burial was taken as the midpoint of published values ( $98.5 \text{ g C m}^{-2} \text{ year}^{-1}$ ; Figure 3; Table 1) derived from two radiometric dating techniques ( $^{210}\text{Pb}$  and  $^{137}\text{Cs}$ :  $87$  and  $110 \text{ g C m}^{-2} \text{ year}^{-1}$ , respectively). It is important to note that burial rates determined here from cores represent a long-term average that may render modern burial rates conservatively low, if SLR is leading to increased accretion. The difference between burial and averaged 4-year NEE equals  $86.5 \text{ g C m}^{-2} \text{ year}^{-1}$  ( $75$  to  $98 \text{ g C m}^{-2} \text{ year}^{-1}$ , using the range in burial rate estimates), in general agreement with direct estimates of lateral flux of  $105.4 \text{ g C m}^{-2} \text{ year}^{-1}$  (Figure 3; Table 1). While the fraction of fixed C (inferred by atmospheric  $\text{CO}_2$  exchange) lost by lat-

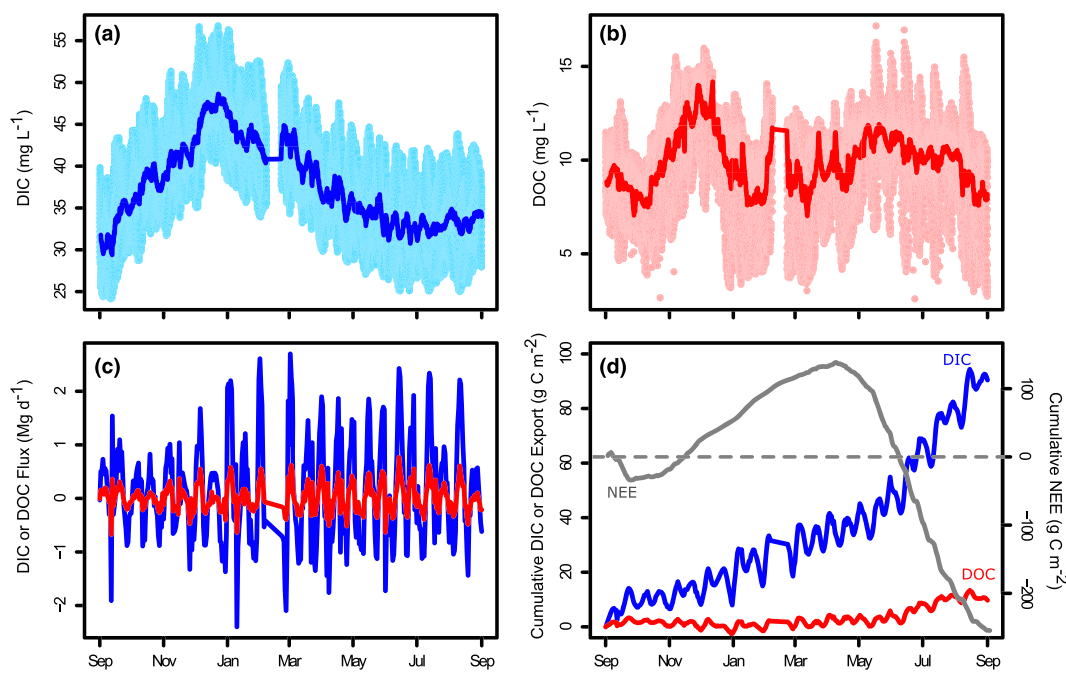


**Figure 2.** Annual time series of aquatic C concentrations and flux from First Mallard Slough for 1 September 2017 to 31 August 2018. (a) Modeled concentrations of dissolved inorganic C (DIC) and (b) dissolved organic C (DOC). In panels a and b, light blue and red points are individual 15 min estimates, and dark blue and red lines are 24 hr moving averages. Daily flux (c) and cumulative annual yields (d) shown as blue and red lines for DIC and DOC, respectively. Cumulative terrestrial net ecosystem exchange (NEE) in panel d denoted by solid gray line. NEE = 0 as horizontal dashed line.

et al., 2008; Cai, 2011; Cai & Wang, 1998; Maher et al., 2018; Wang et al., 2016), suggesting that coastal wetlands should not be considered “efficient” sites of C burial, owing to the large fraction of fixed C lost to the coastal marine environment. Yet it is important to emphasize the fact that although atmospheric C uptake (as NEE) is considerably offset by lateral C fluxes, tidal wetlands still remain larger C sinks than most terrestrial ecosystems.

#### 4.2. Coastal Wetlands Major C Sinks Despite Lateral C Losses

Coastal wetlands are extremely productive, and on the higher end for rates of NEE (Figure 4a). Therefore, despite losing large proportions of fixed C via lateral flux, these systems are still capable of sustaining high rates of annual C burial (Breithaupt et al., 2012; Duarte et al., 2005; Najjar et al., 2018; Wilkinson et al., 2018; Windham-Myers et al., 2018) relative to other terrestrial ecosystem types (Figure 4). The data compilation, arranged by ecosystem type in Figure 4, indicates that coastal wetlands may actually be the ecosystem type for which lateral losses are of greatest relative importance in the NECB, at least when compared on annual timescales. By adding our data (Figure 3) and that from Forbrich et al. (2018) to an existing compilation of global, site-specific NECBs spanning global ecosystem types (Webb et al., 2018), it is clear that a wide range in the fraction of NEE lost via hydrologic export exists among ecosystems (Figure 4a). The few estimates for coastal wetlands show export of ~10% to 90% of fixed C, with a median value of ~39%, near the direct and indirect estimates for our site (Figure 4a; Table 1) and those for tidal marshes spanning the entire U.S. Atlantic Coast (Wang et al., 2016). The median value is also comparable to global estimates of lateral C loss from mangroves (Bouillon, Borges, et al., 2008). This lateral export makes coastal wetlands among the lowest in terms of fraction of fixed C stored, since lateral C export is a larger relative fraction of NEP in tidal wetlands than in inland ecosystems (Figure 4b; Wilcoxon  $p < 0.0001$ ). These results may be broadly representative, given that the coastal sites in our analysis of compiled data sets span a large geographic range and cover distinct biomes (temperate continental, warm Mediterranean, and humid subtropical). This distinction in fraction of NEE lost as lateral export between coastal and inland ecosystems may be due to hydrologic differences related to enhanced exchanges associated with tidal pumping (Wang et al., 2016), which do not

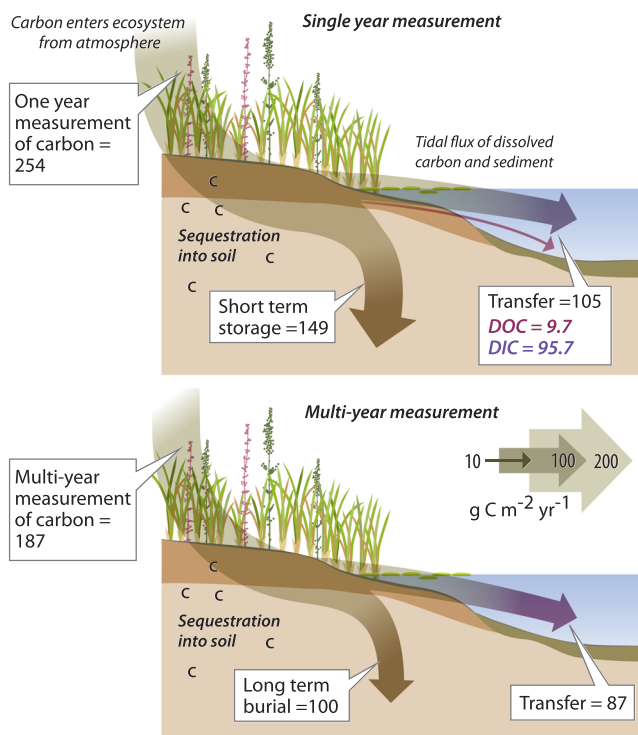


**Figure 3.** Net ecosystem carbon budget (NECB) for the Suisun wetland complex. All values reported in  $\text{g C m}^{-2} \text{ year}^{-1}$ , with arrow sizes scaling with rate of flux (see legend in bottom panel). Single-year direct measurements from 2017–2018 shown in panel a, and longer-term averages from multiyear measurements are shown in panel b. See Table 1 for additional detail; all terms defined in the text.

(between 82.8 and 107.3  $\text{g C m}^{-2} \text{ year}^{-1}$  for DOC + DIC, with 82% to 92% as DIC; Ho et al., 2017) and a tidal marsh in Georgia, USA (156  $\text{g C m}^{-2} \text{ year}^{-1}$  for DIC; Wang & Cai, 2004). Cross-system discrepancies in DIC export may be due to the fact that marsh productivity can vary by an order of magnitude (~150 to 1,600  $\text{g C m}^{-2} \text{ year}^{-1}$ ; Wang et al., 2016, and references therein). With Suisun Marsh generally on the low end of terrestrial net  $\text{CO}_2$  uptake (Table 1), much less fixed C is available for conversion to DIC than at other locations. At the same time, most previous estimates of lateral DIC export must be interpreted with caution, because extrapolations of lateral C fluxes to the annual scale from low-frequency data or time series not covering full spring-neap tidal cycles can have large associated uncertainties (Chu et al., 2018; Downing et al., 2009). For these reasons, DIC fluxes have historically been the most difficult component of the NECB to quantify (Bouillon, Borges, et al., 2008; Ho et al., 2017; Maher et al., 2013, 2018; McLeod et al., 2011; Wang et al., 2016). The MLR modeling approach applied here and elsewhere (Chu et al., 2018; Wang et al., 2016) represents a promising method to better constrain the rates of DIC export from intertidal wetlands and improve our understanding of the composition of, and biogeochemical processes regulating coastal wetland lateral C exports.

#### 4.4. DIC Exports as an Unaccounted Wetland C Sink

Annually, DIC fluxes dramatically exceed those of DOC for the Suisun Marsh complex, which generally aligns with patterns for other coastal environments that have DIC > DOC (Bouillon, Borges, et al., 2008; Ho et al., 2017; Maher et al., 2018; Raymond & Hopkinson, 2003; Wang et al., 2016, 2018). The majority of the DIC lost from Suisun and other coastal wetlands via lateral export (e.g., Figures 3 and 4b) may ultimately be returned to the atmosphere in the form of  $\text{CO}_2$  within the downstream estuarine environment (Borges, 2005; Borges et al., 2003; Ho et al., 2017; Maher et al., 2018; Wang et al., 2018). In this regard, given the lack of appreciable groundwater inputs (see methods), the downstream emission of wetland-derived  $\text{CO}_2$  represents a recycling term of marsh primary productivity, with no net impact on the atmospheric  $\text{CO}_2$  balance (Maher et al., 2018). Yet as marsh DIC moves from an environment with  $\text{pH} \sim 7$  (data not shown), into

occur at the terrestrial-aquatic margins of most inland ecosystems. Effects of infrequent, punctual disturbances that may affect vertical and lateral fluxes are not considered here but potentially alter the relative importance of C storage in ecosystem NECB's over longer timescales. For instance, fires, weather events, and land use change can all impact the balance and magnitude of ecosystem C fluxes (Hayes et al., 2018; Intergovernmental Panel on Climate Change, 2014; Lajtha et al., 2018; Regnier et al., 2013). For coastal wetlands in particular, simulations show that the interactive effect of warming and SLR could actually increase coastal C burial rates in the short term (half-century timescale; Kirwan & Mudd, 2012). Yet habitat loss due to inundation and land development and barriers to wetland migration may offset these influences and liberate soil C through erosion over longer timescales (Chmura, 2013; Hopkinson et al., 2012; IPCC, 2014; Thorne et al., 2018).

#### 4.3. DIC May Dominate Lateral Exports From Coastal Wetlands

The few high-resolution DIC export data sets that currently exist indicate that coastal wetlands export massive quantities of DIC to the marine environment (Bouillon, Borges, et al., 2008; Chu et al., 2018; Wang et al., 2016). These findings also align with the global hypothesis for mangroves that >50% of fixed C may be lost to lateral DIC export (Bouillon, Borges, et al., 2008). The annual DIC flux observed in our study (Figure 3) is lower than estimates of DIC export from other sites globally (from ~400 to >1,000  $\text{g C m}^{-2} \text{ year}^{-1}$ ; Chu et al., 2018; Maher et al., 2018; Santos et al., 2019; Wang et al., 2016, 2018). Instead, our estimates are closer to those from a mangrove/mixed forest catchment in the Florida Everglades

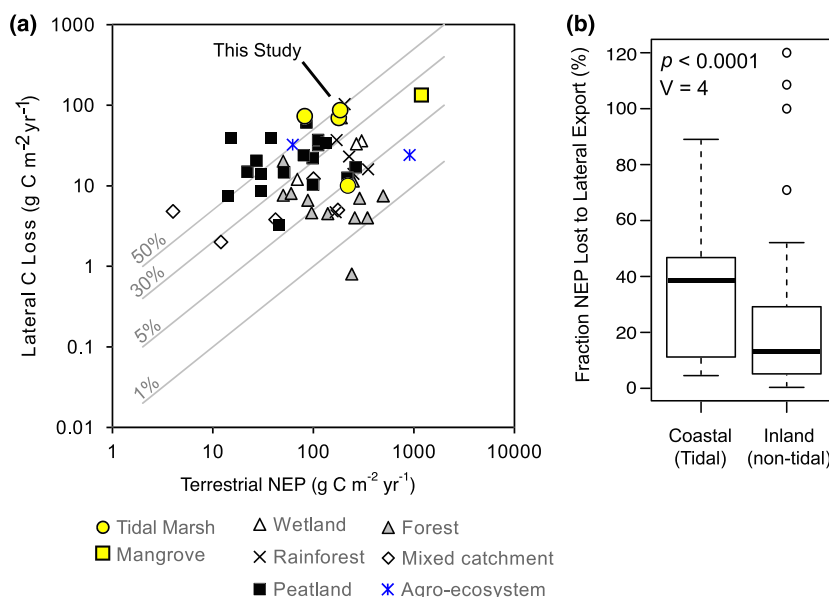


**Figure 4.** Coastal wetlands are among the least efficient ecosystems for storage of fixed C. (a) Compilation of net ecosystem carbon budgets (NECBs) assembled for different terrestrial-aquatic ecosystem types, showing lateral C loss to aquatic systems as a function of terrestrial net ecosystem production (NEP, or net ecosystem exchange, NEE, where  $NEP = -NEE$ ). Coastal habitats are presented as yellow circles (marsh) and squares (mangrove), while inland ecosystems presented in gray scale, and inland agro-ecosystems presented in blue. Solid gray lines denote percent of NEP lost as laterally exported C. (b) Percent of NEP lost as C lateral export, grouped by tidal (i.e., coastal) and nontidal (inland) ecosystem type. Wilcoxon signed-rank test:  $p < 0.0001$ ,  $V = 4$ . All data from Webb et al. (2018) and Forbrich et al. (2018). For consistency with previous work, indirect estimates of lateral flux (Table 1) are shown for Suisun Marsh (this study in panel a).

the marine environment with  $pH > 8$ , the bulk of DIC will be present as  $HCO_3^-$ . Therefore, some fraction of the DIC pool that is exported to the marine environment may be stored in nongaseous form in the ocean over centuries to many millennia (Maher et al., 2018; Millero, 2007). Considerable export of alkalinity from Suisun Marsh at a ratio of  $T_{alk}/DIC$  of  $\sim 0.95$  to 1 (Figures S4a and S4b) indicates that sulfate reduction in marsh soils likely supplies alkalinity (Ho et al., 2017; Sippo et al., 2016) that buffers the downstream environment and will limit the quantity of exported DIC present as free  $CO_2$  that can be degassed to the atmosphere (Maher et al., 2018; Sippo et al., 2016; Wang et al., 2016). Currently, we do not have adequate data to partition the fractions of marsh-derived DIC that is degassed versus retained in the downstream estuarine environment. Yet estimates from other studies have shown that sizeable fractions of marsh- and mangrove-derived DIC may remain in dissolved form upon equilibrium of the DIC pool with the atmosphere (Maher et al., 2018; Neubauer & Anderson, 2003). Previously termed the “marsh  $CO_2$  pump” (Wang et al., 2016; Wang & Cai, 2004), coastal wetland C fixation and DIC export represents an active transfer pathway between reactive (atmospheric) and long-term storage pools (millennial in open ocean; Hansell, 2013; Maher et al., 2018). Ultimately, better accounting for this lateral DIC transfer will help to define the coastal wetland C sequestration efficiency.

#### 4.5. Marsh DOC Fuels Local Heterotrophy Despite Small Estuary-Wide Contribution

The Suisun Marsh NECB developed here helps to address a number of key limitations to understanding coastal zone biogeochemistry and ecology. In particular, DOC export was a comparatively small term in our budget (Table 1; Figure 3). Furthermore, an existing basinwide budget has shown that coastal wetlands in the San Francisco Bay Estuary are a secondary source of organic C relative to riverine exports (Jassby et al., 1993), a conclusion that is consistent for wetlands at the global scale (Bouillon, Borges, et al., 2008; Cai, 2011). The low annual export of DOC observed here (Table 1; Figure 2d) supports this conclusion. Yet it is possible that DOC export rates from distinct wetland complexes may be quite heterogeneous, even within the San Francisco Bay Estuary, since values from Suisun Wetland ( $9.7 \text{ g C m}^{-2} \text{ year}^{-1}$ ; Figure 3;

Table 1) are an order of magnitude lower than indirectly calculated basinwide wetland exports ( $150 \text{ g C m}^{-2} \text{ year}^{-1}$ ) (Jassby et al., 1993). A global compilation supports this conclusion, showing an order of magnitude variability in DOC export from diverse mangrove systems ( $44$  to  $381 \text{ g C m}^{-2} \text{ year}^{-1}$ ) (Bouillon, Borges, et al., 2008). The wide variability in wetland DOC flux estimates underscores the need for multisite empirical data sets, even at the regional scale. Despite this variability, DOC exports are consistently smaller than DIC fluxes across diverse coastal wetland ecosystems (Bouillon, Borges, et al., 2008; Ho et al., 2017; Maher et al., 2018; Santos et al., 2019; Wang et al., 2018), indicating that the dominance of DIC over DOC in the chemical makeup of lateral C exports may be a standard feature of coastal wetland NECBs. Since estuaries are sites of disproportionate  $\text{CO}_2$  outgassing (Cai, 2011; Frankignoulle et al., 1998; Najjar et al., 2018; Volta et al., 2018), it is likely that the mineralization of marsh-derived DOC may play a secondary role in supporting estuarine mineralization and  $\text{CO}_2$  emissions (Cai, 2011; Hopkinson & Smith, 2005; Volta et al., 2018), with our data and other reports (Ho et al., 2017; Neubauer & Anderson, 2003; Santos et al., 2019) showing wetland DIC exports are the dominant pathway by which wetlands likely support estuarine emissions.

Since much of the riverine-derived OC is likely carried past nearshore coastal estuarine zones, marsh DOC exports can importantly sustain heterotrophy and microbial growth in downstream habitats (Cai, 2011; Hopkinson & Smith, 2005), thereby supporting the base of the food web. We confirm such extreme heterotrophy in First Mallard Slough with two lines of evidence. First, in situ plankton respiration rates measured repeatedly over short time intervals from ebb to flooding tide in June used new approaches that minimize bottle containment artifacts to better reflect in situ planktonic processes (Bogard et al., 2019; Pollard, 2013). These rates in First Mallard Slough (mean =  $14.7 \text{ mg O}_2 \text{ L}^{-1} \text{ day}^{-1}$ ; range =  $2.2$  to  $51.4 \text{ mg O}_2 \text{ L}^{-1} \text{ day}^{-1}$ ) greatly exceeded those from a global meta-analysis of estuarine plankton respiration compiled using standard incubation techniques (Hopkinson & Smith, 2005) (cross-site range of  $0.054$  to  $2.69 \text{ mg O}_2 \text{ L}^{-1} \text{ day}^{-1}$ ; comparison based on standard assumption of 1 mole  $\text{CO}_2$  produced per mole  $\text{O}_2$  consumed). Second, the saturation state of aragonite ( $\Omega_a$ ) was consistently  $<<1$  in samples taken during our October 2018 field campaign (Figure S4c), suggesting that intense respiration occurring in marsh soils and the adjacent slough were a dominant feature and major source of  $\text{CO}_2$  to the ecosystem. Though DOC exports are quantitatively small in the ecosystem NECB, they are sufficient to fuel heterotrophy that acidifies the immediate downstream environment, counterbalancing to some degree the alkalinizing influences of anaerobic respiration marsh  $\text{T}_{\text{alk}}$  export (likely dominated by  $\text{SO}_4^{2-}$  reduction; Figure S4a). This dual acidifying and alkalinizing effect of marsh exports on downstream estuarine environments has been highlighted (Wang et al., 2016) and has major implications for our understanding of the role of tidal wetlands in modulating acidification of the coastal ocean (Bauer et al., 2013; Cai, 2011).

## 5. Conclusions

Current appreciation for the role of coastal wetlands as sites of C sequestration (i.e., blue carbon) is likely unimpacted by relatively large hydrologic export rates documented here (Figure 4). The role of coastal wetlands as sites of C-capture and storage is largely based on long-term burial rate estimates that are indeed much greater than for many other global ecosystem types. Instead, the large lateral losses of C from our study site (Figure 3; Table 1) and a handful of other coastal wetlands (Figure 4) underscore the important dual role of these ecosystems as sites of both atmospheric  $\text{CO}_2$  sequestration and C export. The fates of both organic and inorganic C pools exported to the open ocean may be quite distinct, and operating on different time-scales, with implications for coastal wetland roles in short (metabolic OC cycle, return of wetland-derived DIC to the atmosphere) and long (millennial scale ocean DIC storage) timeframes (Maher et al., 2018).

Collectively, our new data provide scalable rates that will help to constrain regional and global coastal C fluxes, a step that is necessary to improve our mechanistic understanding of land-ocean-atmosphere C exchanges, and related issues including coastal hypoxia and acidification. Given the dramatic loss of marsh habitat both in the San Francisco Bay Estuary (~97% habitat reduction; Cloern et al., 2016) and in estuaries around the world (~50% habitat reduction; Hopkinson et al., 2012; Kirwan & Megonigal, 2013), recognizing this dual biogeochemical role that tidal wetlands contribute is especially important in the context of modeling and valuation of marsh restoration and protection efforts.

## Data Availability Statement

All new data are available in the ScienceBase repository (<https://doi.org/10.5066/P9660C55>).

### Acknowledgments

We thank Angela Hansen, Kyle Nakatsuka, Nicholas Graham, and Katie O'Donnell for logistical assistance in the field and the laboratory and Neil Ganju for estimates of wetland flooding extent. We are also grateful for site access and support provided by the Solano Land Trust and by Matt Ferner and the San Francisco Bay National Estuarine Research Reserve. This research was supported by grants to L. W. M. and B. A. B. from the USGS Land Carbon Program. Postdoctoral fellowships from the Delta Science Foundation (to M. J. B. and D. E. B.) and the Natural Sciences and Engineering Research Council of Canada (to MJB) supported this research. This material is based upon work supported by the Delta Stewardship Council Delta Science Program under Grant 5298. The contents of this material do not necessarily reflect the views and policies of the Delta Stewardship Council nor does mention of trade names or commercial products constitute endorsement or recommendation for use. Any use of trade, product, or firm names is for descriptive purposes only and does not imply endorsement by the U.S. Government. The authors thank two anonymous reviewers for helpful comments that improved the manuscript.

### References

Baldocchi, D. D. (2003). Assessing the eddy covariance technique for evaluating carbon dioxide exchange rates of ecosystems: Past, present and future. *Global Change Biology*, 9(4), 479–492. <https://doi.org/10.1046/j.1365-2486.2003.00629.x>

Bandstra, L., Hales, B., & Takahashi, T. (2006). High-frequency measurements of total CO<sub>2</sub>: Method development and first oceanographic observations. *Marine Chemistry*, 100(1–2), 24–38. <https://doi.org/10.1016/j.marchem.2005.10.009>

Barbier, E. B., Hacker, S. D., Kennedy, C., Koch, E. W., Stier, A. C., & Silliman, B. R. (2011). The value of estuarine and coastal ecosystem services. *Ecological Monographs*, 81(2), 169–193. <https://doi.org/10.1890/10-1510.1>

Bauer, J. E., Cai, W. J., Raymond, P. A., Bianchi, T. S., Hopkinson, C. S., & Regnier, P. A. G. (2013). The changing carbon cycle of the coastal ocean. *Nature*, 504(7478), 61–70. <https://doi.org/10.1038/nature12857>

Bergamaschi, B., & Windham-Myers, L. (2018). AmeriFlux US-Srr Suisun marsh - Rush Ranch. <https://doi.org/10.17190/AMF/1418685>

Bergamaschi, B. A., Fleck, J. A., Downing, B. D., Boss, E., Pellerin, B., Ganju, N. K., et al. (2011). Methyl mercury dynamics in a tidal wetland quantified using in situ optical measurements. *Limnology and Oceanography*, 56(4), 1355–1371. <https://doi.org/10.4319/lo.2011.56.4.1355>

Bergamaschi, B. A., Fleck, J. A., Downing, B. D., Boss, E., Pellerin, B. A., Ganju, N. K., et al. (2012). Mercury dynamics in a San Francisco estuary tidal wetland: Assessing dynamics using in situ measurements. *Estuaries and Coasts*, 35(4), 1036–1048. <https://doi.org/10.1007/s12237-012-9501-3>

Bergamaschi, B. A., Kuivila, K. M., & Fram, M. S. (2001). Pesticides associated with suspended sediments entering San Francisco Bay following the first major storm of water year 1996. *Estuaries*, 24(3), 368–380. <https://doi.org/10.2307/1353239>

Bergamaschi, B. A., Krabbenhoft, D. P., Aiken, G. R., Patino, E., Rumbold, D. G., & Orem, W. H. (2012). Tidally driven export of dissolved organic carbon, total mercury, and methylmercury from a mangrove-dominated estuary. *Environmental Science & Technology*, 46(3), 1371–1378. <https://doi.org/10.1021/es2029137>

Boesch, D. F., & Turner, R. E. (1984). Dependence of fishery species on salt marshes: The role of food and refuge. *Estuaries*, 7(4), 460–468. <https://doi.org/10.2307/1351627>

Bogard, M. J., Johnston, S. E., Dornblaser, M. M., Spencer, R. G. M., Striegl, R. G., & Butman, D. E. (2019). Extreme rates and diel variability of planktonic respiration in a shallow sub-arctic lake. *Aquatic Sciences*, 81(4), 60. <https://doi.org/10.1007/s00027-019-0657-9>

Borges, A. V., Djenidi, S., Lacroix, G., Théate, J., Delille, B., & Frankignoulle, M. (2003). Atmospheric CO<sub>2</sub> flux from mangrove surrounding waters. *Geophysical Research Letters*, 30(11), 1558. <https://doi.org/10.1029/2003GL017143>

Borges, A. V. (2005). Do we have enough pieces of the jigsaw to integrate CO<sub>2</sub> fluxes in the coastal ocean? *Estuaries*, 28(1), 3–27. <https://doi.org/10.1007/BF02732750>

Bouillon, S., Connolly, R. M., & Lee, S. Y. (2008). Organic matter exchange and cycling in mangrove ecosystems: Recent insights from stable isotope studies. *Journal of Sea Research*, 59(1–2), 44–58. <https://doi.org/10.1016/j.seares.2007.05.001>

Bouillon, S., Borges, A. V., Castañeda-Moya, E., Diele, K., Dittmar, T., Duke, N. C., et al. (2008). Mangrove production and carbon sinks: A revision of global budget estimates. *Global Biogeochemical Cycles*, 22, GB2013. <https://doi.org/10.1029/2007GB003052>

Bouillon, S., Frankignoulle, M., Dehairs, F., Velimirov, B., Eiler, A., Abril, G., et al. (2003). Inorganic and organic carbon biogeochemistry in the Gautami Godavari estuary (Andhra Pradesh, India) during pre-monsoon: The local impact of extensive mangrove forests. *Global Biogeochemical Cycles*, 17(4), 1114. <https://doi.org/10.1029/2002GB002026>

Breithaupt, J. L., Smoak, J. M., Smith, T. J., Sanders, C. J., & Hoare, A. (2012). Organic carbon burial rates in mangrove sediments: Strengthening the global budget. *Global Biogeochemical Cycles*, 26(3), GB3011. <https://doi.org/10.1029/2012GB004375>

Buchanan, P. A., & Morgan, T. L. (2014). Summary of suspended-sediment concentration data, San Francisco Bay, California, water year 2010: U.S. Geological Survey Data Series 808, 30 p., <https://doi.org/10.3133/ds808>

Butman, D., Stackpoole, S., Stets, E., McDonald, C. P., Clow, D. W., & Striegl, R. G. (2016). Aquatic carbon cycling in the conterminous United States and implications for terrestrial carbon accounting. *Proceedings of the National Academy of Sciences*, 113(1), 58–63. <https://doi.org/10.1073/pnas.1512651112>

Cai, W.-J. (2011). Estuarine and coastal ocean carbon paradox: CO<sub>2</sub> sinks or sites of terrestrial carbon incineration? *Annual Review of Marine Science*, 3(1), 123–145. <https://doi.org/10.1146/annurev-marine-120709-142723>

Cai, W.-J., & Wang, Y. (1998). The chemistry, fluxes, and sources of carbon dioxide in the estuarine waters of the Satilla and Altamaha Rivers, Georgia. *Limnology and Oceanography*, 43(4), 657–668. <https://doi.org/10.4319/lo.1998.43.4.0657>

Callaway, J. C., Borgnis, E. L., Turner, R. E., & Milan, C. S. (2012). Carbon sequestration and sediment accretion in San Francisco Bay tidal wetlands. *Estuaries and Coasts*, 35(5), 1163–1181. <https://doi.org/10.1007/s12237-012-9508-9>

Chapin, F. S., Woodwell, G. M., Randerson, J. T., Rastetter, E. B., Lovett, G. M., Baldocchi, D. D., et al. (2006). Reconciling carbon-cycle concepts, terminology, and methods. *Ecosystems*, 9(7), 1041–1050. <https://doi.org/10.1007/s10021-005-0105-7>

Chmura, G. L. (2013). What do we need to assess the sustainability of the tidal salt marsh carbon sink? *Ocean and Coastal Management*, 83, 25–31. <https://doi.org/10.1016/j.ocecoaman.2011.09.006>

Chu, S. N., Wang, Z. A., Gonanea, M. E., Kroeger, K. D., & Ganju, N. K. (2018). Deciphering the dynamics of inorganic carbon export from intertidal salt marshes using high-frequency measurements. *Marine Chemistry*, 206, 7–18. <https://doi.org/10.1016/j.marchem.2018.08.005>

Cloern, J. E., Robinson, A., Richey, A., Grenier, L., Grossinger, R., Boyer, K. E., et al. (2016). Primary production in the Delta: Then and now. *San Francisco Estuary and Watershed Science*, 14(3). <https://doi.org/10.15447/sfews.2016v14iss3art1>

Dickson, A. G., Sabine, C. L., & Christian, J. R. (2007). Guide to best practices for ocean CO<sub>2</sub> measurements. *PICES Special Publication*, 3. <https://doi.org/10.1039/9781847550835>

Dittmar, T., Hertkorn, N., Kattner, G., & Lara, R. J. (2006). Mangroves, a major source of dissolved organic carbon to the oceans. *Global Biogeochemical Cycles*, 20, GB1012. <https://doi.org/10.1029/2005GB002570>

Dittmar, T., Lara, R. J., & Kattner, G. (2001). River or mangrove? Tracing major organic matter sources in tropical Brazilian coastal waters. *Marine Chemistry*, 73(3–4), 253–271. [https://doi.org/10.1016/S0304-4203\(00\)00110-9](https://doi.org/10.1016/S0304-4203(00)00110-9)

Downing, B. D., Boss, E., Bergamaschi, B. A., Fleck, J. A., Lionberger, M. A., Ganju, N. K., et al. (2009). Quantifying fluxes and characterizing compositional changes of dissolved organic matter in aquatic systems in situ using combined acoustic and optical measurements. *Limnology and Oceanography: Methods*, 7(1), 119–131.

Downing, B. D., Pellerin, B. A., Bergamaschi, B. A., Saraceno, J. F., & Kraus, T. E. C. (2012). Seeing the light: The effects of particles, dissolved materials, and temperature on in situ measurements of DOM fluorescence in rivers and streams. *Limnology and Oceanography: Methods*, 10, 767–775.

Duarte, C. M., Middelburg, J. J., & Caraco, N. (2005). Major role of marine vegetation on the oceanic carbon cycle. *Biogeosciences*, 2(1), 1–8. <https://doi.org/10.5194/bg-2-1-2005>

Duarte, C. M., Losada, I. J., Hendriks, I. E., Mazarrasa, I., & Marbà, N. (2013). The role of coastal plant communities for climate change mitigation and adaptation. *Nature Climate Change*, 3(11), 961–968. <https://doi.org/10.1038/nclimate1970>

Enright, C., Culberson, S. D., & Burau, J. R. (2013). Broad timescale forcing and geomorphic mediation of tidal marsh flow and temperature dynamics. *Estuaries and Coasts*, 36(6), 1319–1339. <https://doi.org/10.1007/s12237-013-9639-7>

Feijtel, T., DeLaune, R., & Patrick, W. (1985). Carbon flow in coastal Louisiana. *Marine Ecology Progress Series*, 24, 255–260. <https://doi.org/10.3354/meps024255>

Forbrich, I., Giblin, A. E., & Hopkinson, C. S. (2018). Constraining marsh carbon budgets using long-term C burial and contemporary atmospheric CO<sub>2</sub> fluxes. *Journal of Geophysical Research: Biogeosciences*, 123, 867–878. <https://doi.org/10.1002/2017JG004336>

Frankignoulle, M., Abril, G., Borges, A., Bourge, I., Canon, C., Delille, B., et al. (1998). Carbon dioxide emission from european estuaries. *Science*, 282(5388), 434–436. <https://doi.org/10.1126/science.282.5388.434>

Ganju, N. K. (2011). A novel approach for direct estimation of fresh groundwater discharge to an estuary. *Geophysical Research Letters*, 38, L11402. <https://doi.org/10.1029/2011GL047718>

Ganju, N. K., Schoellhamer, D. H., & Bergamaschi, B. A. (2005). Suspended sediment fluxes in a tidal wetland: Measurement, controlling factors, and error analysis. *Estuaries*, 28(6), 812–822. <https://doi.org/10.1007/BF02696011>

Hansell, D. A. (2013). Recalculating dissolved organic carbon fractions. *Annual Review of Marine Science*, 5(1), 421–445. <https://doi.org/10.1146/annurev-marine-120710-100757>

Hayes, D. J., Vargas, R., Alin, S., Conant, R. T., Hutyra, L. R., Jacobson, A. R., et al. (2018). The North American carbon budget. In N. Cavallaro et al. (Eds.), *Second State of the Carbon Cycle Report* (Chapt. 2, pp. 71–108). Washington, DC, USA: U.S. Global Change Research Program. <https://doi.org/10.7930/SOCCR2.2018.Ch2>

Ho, D. T., Ferrón, S., Engel, V. C., Anderson, W. T., Swart, P. K., Price, R. M., & Barbero, L. (2017). Dissolved carbon biogeochemistry and export in mangrove-dominated rivers of the Florida Everglades. *Biogeosciences*, 14(9), 2543–2559. <https://doi.org/10.5194/bg-14-2543-2017>

Hopkinson, C. S., Cai, W.-J., & Hu, X. (2012). Carbon sequestration in wetland dominated coastal systems—A global sink of rapidly diminishing magnitude. *Current Opinion in Environmental Sustainability*, 4(2), 186–194. <https://doi.org/10.1016/j.cosust.2012.03.005>

Hopkinson, C. S., & Smith, E. M. (2005). Estuarine respiration: An overview of benthic, pelagic, and whole system respiration. In P. A. del Giorgio, P. J. Le, & B. Williams (Eds.), *Respiration in Aquatic Ecosystems* (Chap. 8, pp. 122–146). New York: Oxford University Press. <https://doi.org/10.1093/acprof:oso/9780198527084.003.0008>

Jassby, A., Cloern, J., & Powell, T. (1993). Organic carbon sources and sinks in San Francisco Bay: Variability induced by river flow. *Marine Ecology Progress Series*, 95(1–2), 39–54. <https://doi.org/10.3354/meps095039>

Johnson, J. B., & Omland, K. S. (2004). Model selection in ecology and evolution. *Trends in Ecology & Evolution*, 19(2), 101–108. <https://doi.org/10.1016/j.tree.2003.10.013>

Kirwan, M. L., & Megonigal, J. P. (2013). Tidal wetland stability in the face of human impacts and sea-level rise. *Nature*, 504(7478), 53–60. <https://doi.org/10.1038/nature12856>

Kirwan, M. L., & Mudd, S. M. (2012). Response of salt-marsh carbon accumulation to climate change. *Nature*, 489(7417), 550–553. <https://doi.org/10.1038/nature11440>

Knox, S. H., Windham-Myers, L., Anderson, F., Sturtevant, C., & Bergamaschi, B. (2018). Direct and indirect effects of tides on ecosystem-scale CO<sub>2</sub> exchange in a brackish tidal marsh in northern California. *Journal of Geophysical Research: Biogeosciences*, 123, 787–806. <https://doi.org/10.1002/2017JG004048>

Lajtha, K., Bailey, V. L., McFarlane, K., Paustian, K., Bachelet, D., Abramoff, R., et al. (2018). Chapter 12: Soils. In N. Cavallaro et al. (Eds.). Washington, DC, USA: U.S. Global Change Research Program. <https://doi.org/10.7930/SOCCR2.2018.Ch12>

Legendre, P. (2013). Package ‘lmodel2’. Model II Regression, *Version 1*.

Maher, D. T., Santos, I. R., Golby-Smith, L., Gleeson, J., & Eyre, B. D. (2013). Groundwater-derived dissolved inorganic and organic carbon exports from a mangrove tidal creek: The missing mangrove carbon sink? *Limnology and Oceanography*, 58(2), 475–488. <https://doi.org/10.4319/lo.2013.58.2.0475>

Maher, D. T., Call, M., Santos, I. R., & Sanders, C. J. (2018). Beyond burial: Lateral exchange is a significant atmospheric carbon sink in mangrove forests. *Biology Letters*, 14(7), 20180200. <https://doi.org/10.1098/rsbl.2018.0200>

McLeod, E., Chmura, G. L., Bouillon, S., Salm, R., Björk, M., Duarte, C. M., et al. (2011). A blueprint for blue carbon: Toward an improved understanding of the role of vegetated coastal habitats in sequestering CO<sub>2</sub>. *Frontiers in Ecology and the Environment*, 9(10), 552–560. <https://doi.org/10.1890/110004>

Millero, F. J. (2007). The marine inorganic carbon cycle. *Chemical Reviews*, 107(2), 308–341. <https://doi.org/10.1021/cr0503557>

Moffat, A. M., Papale, D., Reichstein, M., Hollinger, D. Y., Richardson, A. D., Barr, A. G., et al. (2007). Comprehensive comparison of gap-filling techniques for eddy covariance net carbon fluxes. *Agricultural and Forest Meteorology*, 147(3–4), 209–232. <https://doi.org/10.1016/j.agrformet.2007.08.011>

Najjar, R. G., Herrmann, M., Alexander, R., Boyer, E. W., Burdige, D. J., Butman, D., et al. (2018). Carbon budget of tidal wetlands, estuaries, and shelf waters of eastern North America. *Global Biogeochemical Cycles*, 32, 389–416. <https://doi.org/10.1002/2017GB005790>

Nellemann, C., Corcoran, E., Duarte, C. M., Valdés, L., DeYoung, C., Fonseca, L., & Grimsditch, G. (2009). Blue carbon: The role of healthy oceans in binding carbon. GRID-Arendal: United Nations Environment Programme. Retrieved from <https://portals.iucn.org/library/node/9442>

Neubauer, S. C., & Anderson, I. C. (2003). Transport of dissolved inorganic carbon from a tidal freshwater marsh to the York River estuary. *Limnology and Oceanography*, 48(1 I), 299–307. <https://doi.org/10.4319/lo.2003.48.1.0299>

Pollard, P. C. (2013). In situ rapid measures of total respiration rate capture the super labile DOC bacterial substrates of freshwater. *Limnology and Oceanography: Methods*, 11(11), 584–593. <https://doi.org/10.4319/lom.2013.11.584>

Raymond, P. A., & Hopkinson, C. S. (2003). Ecosystem modulation of dissolved carbon age in a temperate marsh-dominated estuary. *Ecosystems*, 6(7), 694–705. <https://doi.org/10.1007/s10021-002-0213-6>

R-development-core-team (2017). *R: A language and environment for statistical computing. R Foundation for Statistical Computing*. Vienna: R Foundation for Statistical Computing. <https://doi.org/10.1007/978-3-540-74686-7>

Regnier, P., Friedlingstein, P., Ciais, P., Mackenzie, F. T., Gruber, N., Janssens, I. A., et al. (2013). Anthropogenic perturbation of the carbon fluxes from land to ocean. *Nature Geoscience*, 6(8), 597–607. <https://doi.org/10.1038/ngeo1830>

Santos, I. R., Webb, J. R., Maher, D. T., Sanders, C. J., & Larkin, R. (2019). Carbon outwelling and outgassing vs. burial in an estuarine tidal creek surrounded by mangrove and saltmarsh wetlands. *Limnology and Oceanography*. <https://doi.org/10.1002/lno.11090>

Saraceno, J. F., Shanley, J. B., Downing, B. D., & Pellerin, B. A. (2017). Clearing the waters: Evaluating the need for site-specific field fluorescence corrections based on turbidity measurements. *Limnology and Oceanography: Methods*, 15(4), 408–416. <https://doi.org/10.1002/lom3.10175>

Sippo, J. Z., Maher, D. T., Tait, D. R., Holloway, C. J., Santos, I. R., & Holloway, C. (2016). Are mangroves drivers or buffers of coastal acidification? Insights from alkalinity and dissolved inorganic carbon export estimates across a latitudinal transect. *Global Biogeochemical Cycles*, 30, 753–766. <https://doi.org/10.1002/2015GB005324>

Intergovernmental Panel on Climate Change (IPCC) (2014). Summary for Policymakers. In *Climate Change 2013 – The Physical Science Basis: Working Group I Contribution to the Fifth Assessment Report of the Intergovernmental Panel on Climate Change* (pp. 1–30). Cambridge: Cambridge University Press. <https://doi.org/10.1017/CBO9781107415324.004>

Tank, S. E., Frey, K. E., Striegl, R. G., Raymond, P. a., Holmes, R. M., McClelland, J. W., & Peterson, B. J. (2012). Landscape-level controls on dissolved carbon flux from diverse catchments of the circumboreal. *Global Biogeochemical Cycles*, 26, GB0E02. <https://doi.org/10.1029/2012GB004299>

Thorne, K., MacDonald, G., Guntenspergen, G., Ambrose, R., Buffington, K., Dugger, B., et al. (2018). U.S. Pacific coastal wetland resilience and vulnerability to sea-level rise. *Science Advances*, 4(2), eaao3270. <https://doi.org/10.1126/sciadv.aao3270>

Troxler, T. (2013). Integrated carbon budget models for the Everglades terrestrial-coastal-oceanic gradient: Current status and needs for inter-site comparisons. *Oceanography*, 26(3), 98–107. <https://doi.org/10.5670/oceanog.2013.51>

Volta, C., Ho, D. T., Friederich, G., Engel, V. C., & Bhat, M. (2018). Influence of water management and natural variability on dissolved inorganic carbon dynamics in a mangrove-dominated estuary. *Science of the Total Environment*, 635, 479–486. <https://doi.org/10.1016/j.scitotenv.2018.04.088>

Waldbusser, G. G., Hales, B., Langdon, C. J., Haley, B. A., Schrader, P., Brunner, E. L., et al. (2015). Ocean acidification has multiple modes of action on bivalve larvae. *PLoS ONE*, 10(6), e0128376. <https://doi.org/10.1371/journal.pone.0128376>

Wang, S. R., Di Iorio, D., Cai, W. J., & Hopkinson, C. S. (2018). Inorganic carbon and oxygen dynamics in a marsh-dominated estuary. *Limnology and Oceanography*, 63(1), 47–71. <https://doi.org/10.1002/lno.10614>

Wang, Z. A., & Cai, W.-J. (2004). Carbon dioxide degassing and inorganic carbon export from a marsh-dominated estuary (the Duplin River): A marsh CO<sub>2</sub> pump. *Limnology and Oceanography*, 49(2), 341–354. <https://doi.org/10.4319/lo.2004.49.2.020341>

Wang, Z. A., Kroeger, K. D., Ganju, N. K., Gonanea, M. E., & Chu, S. N. (2016). Intertidal salt marshes as an important source of inorganic carbon to the coastal ocean. *Limnology and Oceanography*, 61(5), 1916–1931. <https://doi.org/10.1002/lno.10347>

Webb, J. R., Santos, I. R., Maher, D. T., & Finlay, K. (2018). The importance of aquatic carbon fluxes in net ecosystem carbon budgets: A catchment-scale review. *Ecosystems*, 22(3), 508–527. <https://doi.org/10.1007/s10021-018-0284-7>

Wilkinson, G. M., Besterman, A., Buelo, C., Gephart, J., & Pace, M. L. (2018). A synthesis of modern organic carbon accumulation rates in coastal and aquatic inland ecosystems. *Scientific Reports*, 8(1), 15736. <https://doi.org/10.1038/s41598-018-34126-y>

Windham-Myers, L., Cai, W.-J., Alin, S. R., Andersson, A., Crosswell, J., Dunton, K. H., et al. (2018). Tidal wetlands and estuaries. In N. Cavallaro (Eds.), *Second State of the Carbon Cycle Report (SOCCR2): A Sustained Assessment Report* (Chap. 15, pp. 596–648). Washington, DC, USA: U.S. Global Change Research Program. <https://doi.org/10.7930/SOCCR2.2018.Ch15>

Worm, B., Selkoe, K. A., Jackson, J. B. C., Lotze, H. K., Stachowicz, J. J., Beaumont, N., et al. (2006). Impacts of biodiversity loss on ocean ecosystem services. *Science*, 314(5800), 787–790. <https://doi.org/10.1126/science.1132294>

Xiao, D., Deng, L., Kim, D., Huang, C., & Tian, K. (2019). Carbon budgets of wetland ecosystems in China. *Global Change Biology*, 25(6), 2061–2076. <https://doi.org/10.1111/gcb.14621>